Letter

$\mathcal{PT}$-phase diagram with quantum jump in a non-Hermitian photonic structure

Xinchen Zhang,[1] Yun Ma,[1,*] Qi Liu,[1,2] Nuo Wang,[1] Yali Jia,[1] Qi Zhang,[1,3] Zhanqiang Bai,[4] Junxiang Zhang,[5] Qihuang Gong,[1,2,6,7,8] and Ying Gu[1,2,6,7,8,†]

[1]*State Key Laboratory for Mesoscopic Physics, Department of Physics, Peking University, Beijing 100871, China*
[2]*Frontiers Science Center for Nano-optoelectronics & Collaborative Innovation Center of Quantum Matter & Beijing Academy of Quantum Information Sciences, Peking University, Beijing 100871, China*
[3]*Institute of Navigation and Control Technology, China North Industries Group Corporation, Beijing 100089, China*
[4]*School of Mathematical Sciences, Soochow University, Suzhou 215006, China*
[5]*Zhejiang Province Key Laboratory of Quantum Technology and Device, Department of Physics, Zhejiang University, Hangzhou 310027, China*
[6]*Collaborative Innovation Center of Extreme Optics, Shanxi University, Taiyuan, Shanxi 030006, China*
[7]*Peking University Yangtze Delta Institute of Optoelectronics, Nantong 226010, China*
[8]*Hefei National Laboratory, Hefei 230088, China*

(Received 6 September 2023; accepted 1 April 2024; published 19 April 2024)

Quantum jumps induced by gain and loss have different quantum behaviors in non-Hermitian photonics. However, the jump effect on global quantum $\mathcal{PT}$ properties has not been comprehensively understood yet. Here, with considering quantum jump of loss and gain in a photonic dimer structure, we analytically obtained the $\mathcal{PT}$-phase diagram under the steady-state condition and defined a Hermitian exchange operator to characterize the $\mathcal{PT}$-symmetry or -broken phase. When we input Fock states into a $\mathcal{PT}$-broken bi-waveguide splitting system, most photons will concentrate in the dominant waveguide with some state distributions. Especially in Hong-Ou-Mandel interferences, if gain is added, whether loss exists or not, $g^{(2)}$ is always larger than zero because loss cannot compensate gain as their different quantum jump effects. The quantum $\mathcal{PT}$-phase diagram paves the way to the quantum state engineering, quantum interferences, and logic operations in non-Hermitian photonic systems.

DOI: 10.1103/PhysRevA.109.L041503

Introduction. An open quantum system generally exchanges the energy with the external environment, i.e., it is non-Hermitian. With varying some specific parameters in a non-Hermitian parity-time ($\mathcal{PT}$) system, there exist exceptional points (EPs) from $\mathcal{PT}$ symmetry to broken, where the eigenvalues and corresponding eigenvectors simultaneously coalesce [1]. Various theoretical works related to $\mathcal{PT}$ symmetry are proposed [2–4], exhibiting some interesting phenomena, such as optical solitons and Bloch oscillations in periodical potentials [5,6], edge-gain effect, and gain-loss-induced skin modes in topological systems [7,8]. Simultaneously, $\mathcal{PT}$ symmetry and broken behaviors are experimentally realized in atomic and trapped ion systems [9,10], acoustic medium [11], electronic circuit [12], photonic lattice [13], and quantum optical systems [14–16].

In addition to the above-mentioned systems, photonic structures are good candidates to realize $\mathcal{PT}$ symmetry or broken through modulating the refractive index or gain and loss [17,18]. Owing to the similarity between the Schrödinger equation and the paraxial optical equation [19], photonic structures have an inherent advantage for realizing $\mathcal{PT}$ symmetry. Both optical waveguides [20,21] and whispering gallery microcavities [22,23] can construct a $\mathcal{PT}$-symmetric system by two-mode coupling with gain and loss. Besides, $\mathcal{PT}$ symmetry has been observed in metasurface [24] and periodically modulated refractive index material [25,26]. Because of the nonreciprocal property in $\mathcal{PT}$-broken and enhanced sensitivity at EPs, $\mathcal{PT}$-symmetric optics can be applied in optical isolation devices [22], sensing [27], laser [28,29], and chiral optics [30].

However, previous studies on $\mathcal{PT}$-symmetric photonic structures are almost limited to classical optics, where loss and gain in the same mode can cancel each other and thereby be considered as an average effect, while in a quantum $\mathcal{PT}$ system, the role of loss and gain is different: the gain while generating photons will bring some noise, but the loss while annihilating photons cannot lower any noise and can even cause vacuum noise. These two irreversible processes inevitably produce different kinds of quantum jump, leading to some interesting quantum behaviors. With the consideration of quantum jump, people studied the saturation effects on the noise and entanglement [31,32], the positions and characteristic of EPs [33,34], and the switching between $\mathcal{PT}$ and anti-$\mathcal{PT}$ systems [35] in non-Hermitian gain-loss coupled cavities. Quantum correlations of a $\mathcal{PT}$-symmetric system with quantum jump have also been studied recently [36]. But all these works did not focus on the different kinds of quantum jump of gain and loss. Until now, with quantum jump, there is

*ma_yun@pku.edu.cn
†ygu@pku.edu.cn

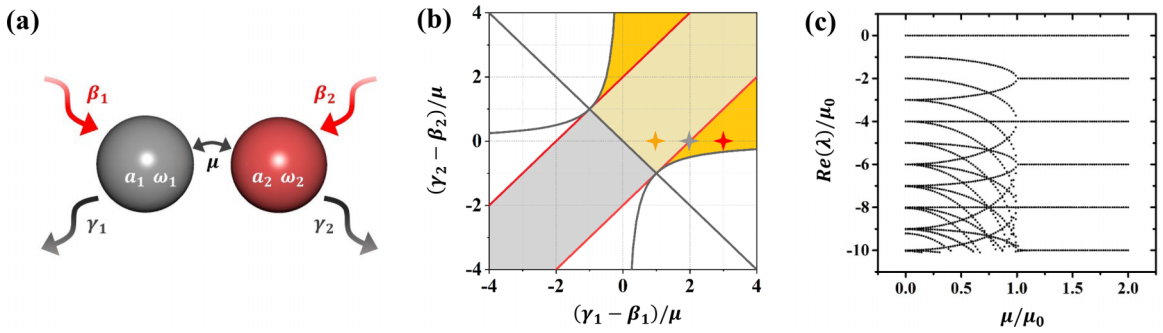

FIG. 1. (a) Schematic diagram of photonic dimer structures with coupling coefficient μ and loss rate γ_j and gain rate β_j for $j = 1, 2$. (b) $\mathcal{PT}$-phase diagram with steady-state regime. EPs satisfying $(\beta_1 - \gamma_1)/\mu - (\beta_2 - \gamma_2)/\mu = \pm 2$ are shown as two red parallel diagonal lines. The regime between two EP lines is $\mathcal{PT}$ symmetry, while outside of EP lines is $\mathcal{PT}$ broken. The yellow part is the steady-state regime. Left yellow star: $\mathcal{PT}$ symmetry; middle gray star: EP; right red star: $\mathcal{PT}$ broken. (c) Real parts of eigenvalues of Liouvillian $\mathcal{L}(\mu)$ with the EP at $\mu = \mu_0$. Here $\gamma_1 = 3.1\mu_0$, $\beta_1 = 0.1\mu_0$, $\gamma_2 = 1.1\mu_0$, and $\beta_2 = 0.1\mu_0$.

no panoptic study on the behavior of full gain-loss parameter space, i.e., the quantum $\mathcal{PT}$-phase diagram. Once this phase diagram is obtained, people can use photonic structures to engineer the quantum state and to realize the quantum logic operation, especially when $\mathcal{PT}$ symmetry is broken.

In this Letter, we analytically obtain the quantum phase diagram of $\mathcal{PT}$ symmetry or broken in photonic dimer cavities with both gain and loss simultaneously existing [Fig. 1(a)]. For the consideration of reality, the steady-state regime under the weak gain is identified. To characterize the transition from $\mathcal{PT}$ symmetry to broken, we define the exchange operator with exchanging the quadrature variables between two modes. Then, we explore the quantum splitting behaviors with discrete variable of several photons. If inputting Fock states into a $\mathcal{PT}$-broken bi-waveguide splitting system, most photons concentrate in the dominant waveguide with some state distributions. Especially in Hong-Ou-Mandel (HOM) interferences, if gain is added, whether loss exists or not, $g^{(2)}$ is always larger than zero because loss cannot compensate gain as their different quantum jump effects. The phase diagram with full parameter space is the basis to study the quantum state fabrication, quantum interferences, and logic operations in non-Hermitian quantum photonic systems.

Quantum $\mathcal{PT}$-phase diagram with steady-state regime. Consider photonic dimer cavities with loss and gain simultaneously existing [Fig. 1(a)], when we let $\omega_1 = \omega_2 = \omega$, whose Hamiltonian is

$$\hat{H} = \hbar\omega\hat{a}_1^\dagger\hat{a}_1 + \hbar\omega\hat{a}_2^\dagger\hat{a}_2 + \hbar\mu(\hat{a}_1^\dagger\hat{a}_2 + \hat{a}_2^\dagger\hat{a}_1), \tag{1}$$

where $\hat{a}_j$ and $\hat{a}_j^\dagger$ $(j = 1, 2)$ are the boson annihilation and creation operator, respectively, and μ is the coupling strength between two cavities. With the weak gain and weak incident light, the gain saturation effect can be neglected [37]. Then the non-Hermitian system is governed by the Lindblad master equation [38],

$$\frac{d\hat{\rho}}{dt} = -\frac{i}{\hbar}[\hat{H}, \hat{\rho}] + \sum_{j=1,2} \gamma_j(2\hat{a}_j\hat{\rho}\hat{a}_j^\dagger - \hat{\rho}\hat{a}_j^\dagger\hat{a}_j - \hat{a}_j^\dagger\hat{a}_j\hat{\rho}) + \sum_{j=1,2} \beta_j(2\hat{a}_j^\dagger\hat{\rho}\hat{a}_j - \hat{\rho}\hat{a}_j\hat{a}_j^\dagger - \hat{a}_j\hat{a}_j^\dagger\hat{\rho}), \tag{2}$$

where γ_j (β_j) is the loss (gain) coefficient of the jth cavity. The quantum jumps $\gamma_j(2\hat{a}_j\hat{\rho}\hat{a}_j^\dagger)$ and $\beta_j(2\hat{a}_j^\dagger\hat{\rho}\hat{a}_j)$ originate from loss and gain, respectively, whose quantum behaviors are totally different [39]. While in classical $\mathcal{PT}$ systems [21], these two effects are seen as an average through gain to compensate a loss (such as the scattering and absorption).

To construct the quantum $\mathcal{PT}$-phase diagram, based on Eq. (2), we derive the evolution of $\langle\hat{a}_1\rangle$ and $\langle\hat{a}_2\rangle$ with varying t [40],

$$i\frac{d}{dt}\begin{pmatrix}\langle\hat{a}_1\rangle\\ \langle\hat{a}_2\rangle\end{pmatrix} = H_{\text{eff}}\begin{pmatrix}\langle\hat{a}_1\rangle\\ \langle\hat{a}_2\rangle\end{pmatrix}, \tag{3}$$

where

$$H_{\text{eff}} = \begin{pmatrix}\omega - i\gamma_1 + i\beta_1 & \mu\\ \mu & \omega - i\gamma_2 + i\beta_2\end{pmatrix}. \tag{4}$$

The eigenvalues of H_{eff} are

$$\omega_\pm = \omega - \frac{i}{2}(\gamma_1 - \beta_1 + \gamma_2 - \beta_2) \pm \frac{1}{2}\sqrt{4\mu^2 - [(\gamma_1 - \beta_1) - (\gamma_2 - \beta_2)]^2}. \tag{5}$$

The degeneracy parts of eigenvalues $\omega_\pm$, which satisfy $(\gamma_1 - \beta_1)/\mu - (\gamma_2 - \beta_2)/\mu = \pm 2$, are called EP lines, shown as two red lines in the $\mathcal{PT}$-phase diagram [Fig. 1(b)]. The area between two red lines is $\mathcal{PT}$ symmetric, while the areas outside these two lines are $\mathcal{PT}$ broken. In a classical $\mathcal{PT}$-phase diagram, one point corresponds to only one set of parameters [41], while in a quantum $\mathcal{PT}$-phase diagram, owing to quantum jump effects, each point [see yellow, gray, or red star in Fig. 1(b)] corresponds to infinite sets of parameters. Furthermore, all sets of these parameters in this point share the common $\mathcal{PT}$-symmetric properties.

On the other hand, Eq. (2) can be written as $\frac{d\hat{\rho}}{dt} = \mathcal{L}\hat{\rho}$ with the Liouvillian operator $\mathcal{L}$. Given a set of complete quantum state basis vectors, $\mathcal{L}$ can be expressed as a high dimension matrix. Figure 1(c) shows the real parts of eigenvalues of Liouvillian $\mathcal{L}(\mu)$ with $\gamma_1 = 3.1\mu_0$, $\beta_1 = 0.1\mu_0$, $\gamma_2 = 1.1\mu_0$, and $\beta_2 = 0.1\mu_0$, respectively. One can see that the splitting point locating at $\mu = \mu_0$ is identical to the gray star in the phase diagram [Fig. 1(b)]. More details about $\mathcal{L}$ are shown in Ref. [40].

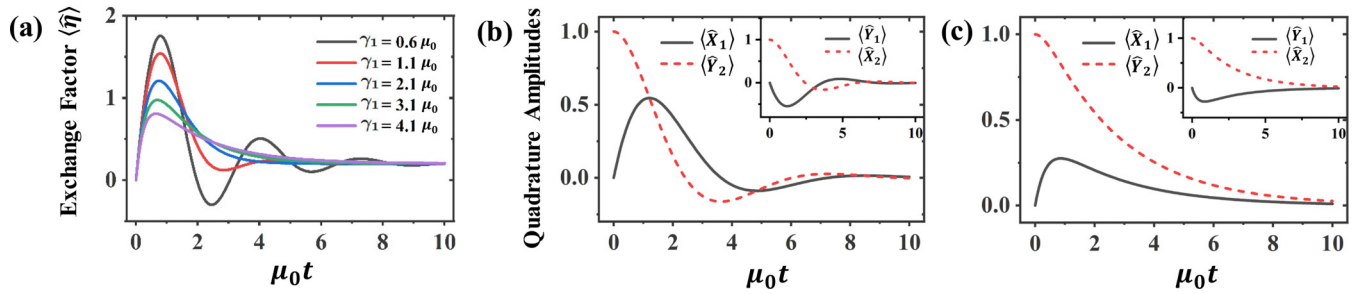

FIG. 2. (a) Evolution of $\langle\hat{\eta}\rangle$ with varying γ_1. The exchange between $\langle\hat{X}_1\rangle$ and $\langle\hat{Y}_2\rangle$ (inset: $\langle\hat{X}_2\rangle$ and $\langle\hat{Y}_1\rangle$) (b) in $\mathcal{PT}$ symmetry with $\gamma_1 = 1.1\mu_0$ [yellow star in Fig. 1(b)] and (c) in $\mathcal{PT}$ broken with $\gamma_1 = 3.1\mu_0$ [red star in Fig. 1(b)]. The initial state is $|0, \alpha = 1 + i\rangle$ and other parameters are $\beta_1 = 0.1\mu_0$, $\gamma_2 = 0.1\mu_0$, $\beta_2 = 0.1\mu_0$, and $\mu = \mu_0$.

Furthermore, the evolution of the mean photon number $\langle\hat{n}_1\rangle = \langle\hat{a}_1^\dagger\hat{a}_1\rangle$, $\langle\hat{n}_2\rangle = \langle\hat{a}_2^\dagger\hat{a}_2\rangle$ of two modes, and an exchange factor $\langle\hat{\eta}\rangle = \langle i(\hat{a}_2^\dagger\hat{a}_1 - \hat{a}_1^\dagger\hat{a}_2)\rangle$ can be written as [40]

$$\begin{aligned}
\frac{d}{dt}\langle\hat{n}_1\rangle &= 2(\beta_1 - \gamma_1)\langle\hat{n}_1\rangle + \mu\langle\hat{\eta}\rangle + 2\beta_1,\\
\frac{d}{dt}\langle\hat{n}_2\rangle &= 2(\beta_2 - \gamma_2)\langle\hat{n}_2\rangle - \mu\langle\hat{\eta}\rangle + 2\beta_2,\\
\frac{d}{dt}\langle\hat{\eta}\rangle &= 2\mu\langle\hat{n}_2\rangle - 2\mu\langle\hat{n}_1\rangle + (\beta_1 + \beta_2 - \gamma_1 - \gamma_2)\langle\hat{\eta}\rangle, \quad (6)
\end{aligned}$$

whose solutions satisfy the steady-state conditions that both $\gamma_1 + \gamma_2 - \beta_1 - \beta_2 > 0$ and $(\gamma_1 - \beta_1)(\gamma_2 - \beta_2) + \mu^2 > 0$, shown as the yellow area of the phase diagram in Fig. 1(b). Under steady-state conditions, the final values of the mean photon number of two modes as well as $\langle\hat{\eta}\rangle$ can be written as [40] $\langle\hat{n}_1\rangle_{ss} = [\Delta_1 - \beta_1(\Delta_2 + 2\beta_2\gamma_2 - \gamma_2^2)]/\Delta_3$, $\langle\hat{n}_2\rangle_{ss} = [\Delta_1 - \beta_2(\Delta_2 + 2\beta_1\gamma_1 - \gamma_1^2)]/\Delta_3$, and $\langle\hat{\eta}\rangle_{ss} = 2\mu(\beta_2\gamma_1 - \beta_1\gamma_2)/\Delta_3$, with $\Delta_1 = (\beta_1 + \beta_2)(\beta_1\beta_2 + \mu^2)$, $\Delta_2 = \beta_1\gamma_2 + \beta_2\gamma_1 - \gamma_1\gamma_2$, and $\Delta_3 = (\gamma_1 + \gamma_2 - \beta_1 - \beta_2)[(\gamma_1 - \beta_1)(\gamma_2 - \beta_2) + \mu^2]$. One can see that, for one steady-state point, there are infinite sets of parameters γ_1, β_1, γ_2, and β_2 corresponding to infinite steady-state values. But owing to the decoherence effects of loss and gain, the steady state will finally become a thermal state without any quantum feature [40]. Our following discussions are limited within the steady-state regime.

Exchange operator to characterize the $\mathcal{PT}$ phase. To characterize the $\mathcal{PT}$ symmetry or broken, we rewrite the exchange operator $\hat{\eta}$ as

$$\hat{\eta} = 2(\hat{X}_1\hat{Y}_2 - \hat{X}_2\hat{Y}_1), \quad (7)$$

with $\hat{X}_{1,2} = (\hat{a}_{1,2} + \hat{a}_{1,2}^\dagger)/2$ and $\hat{Y}_{1,2} = (\hat{a}_{1,2} - \hat{a}_{1,2}^\dagger)/2i$. $\hat{\eta}$, as a Hermitian operator, expresses the exchange between quadrature variables $\hat{X}_{1,2}$ and $\hat{Y}_{2,1}$. Its expectation value $\langle\hat{\eta}\rangle$ is a real number called the exchange factor. Figure 2(a) gives the evolution of $\langle\hat{\eta}\rangle$ with varying the loss rate γ_1. Here, $\beta_1 = 0.1\mu_0$, $\gamma_2 = 0.1\mu_0$, $\beta_2 = 0.1\mu_0$, and $\mu = \mu_0$, where $\mu_0 = 10^{10}$ Hz, and the initial state is a coherent state $|0, \alpha = 1 + i\rangle$. From Fig. 2(a), $\langle\hat{\eta}\rangle$ experiences the phase transition from $\mathcal{PT}$ symmetry at $\gamma_1 = 1.1\mu_0$, via the EP point at $\gamma_1 = 2.1\mu_0$, to $\mathcal{PT}$ broken at $\gamma_1 = 3.1\mu_0$, corresponding to the yellow, gray, and red stars in Fig. 1(b), respectively. When $\mathcal{PT}$ symmetry is unbroken, $\langle\hat{\eta}\rangle$ oscillates with t. In contrast, when $\mathcal{PT}$ symmetry is broken, $\langle\hat{\eta}\rangle$ monotonically decreases after a rise and then comes to the steady state. Through calculating $\langle\hat{\eta}\rangle$ with varying the parameters in the same point, it is found that their global properties (i.e., symmetric, EP, and broken) are not changed [40].

For any value of γ_1, $\langle\hat{\eta}\rangle$ is approaching the same value with $t \to \infty$, just for a specific case $\gamma_2 = \beta_2$.

Correspondingly, we explore the exchanging processing between quadrature amplitudes $\langle\hat{X}_{1,2}\rangle$ and $\langle\hat{Y}_{2,1}\rangle$. For the $\mathcal{PT}$ symmetry, there is an exchange between $\langle\hat{X}_{1,2}\rangle$ and $\langle\hat{Y}_{2,1}\rangle$with $\gamma_1 = 1.1\mu_0$ [Fig. 2(b)]. In contrast, when $\mathcal{PT}$ is broken, they decay exponential with $\langle\hat{X}_1\rangle < \langle\hat{Y}_2\rangle$ and $\langle\hat{Y}_1\rangle < \langle\hat{X}_2\rangle$ with $\gamma_1 = 3.1\mu_0$ [Fig. 2(c)]. If now we input the Fock state $|m, n\rangle$ as an initial state, $\langle\hat{X}_{1,2}\rangle$ and $\langle\hat{Y}_{2,1}\rangle$ will be 0 for all the time [40]. So if only inputting Fock states, one cannot use the exchange of quadrature amplitudes to distinguish the $\mathcal{PT}$-symmetry or -broken phase, while, whatever for Fock states or coherent states, one can clearly distinguish them through $\langle\hat{\eta}\rangle$ [40]. Therefore, exchange operator $\hat{\eta}$ can fully characterize the properties of $\mathcal{PT}$ symmetry or the broken in quantum photonic system.

Engineering quantum state with $\mathcal{PT}$ broken. The above theory can be applied to non-Hermitian beam splitters [42], which have some unique properties and applications, such as quantum coherent perfect absorption [43], antibunching of bosons [44], and fabrication of multibit quantum gates [45]. Now, let us take a coupled waveguide system as an example to study the quantum state engineering. Shown as Figs. 3(a) and 3(b), two gain-loss waveguides with coupled distance L can be seen as a beam splitter. If L is too short, the interaction between two modes is not enough. In contrast, if L is too long, any input quantum state will become a thermal state. Thus there exists an optimal interval of L to balance the quantum coherence and $\mathcal{PT}$-symmetry effects. When $\gamma_1 = 1.1\mu_0 \sim 3.1\mu_0$, $\beta_1 = 0.1\mu_0$, $\gamma_2 = 0.1\mu_0$, $\beta_2 = 0.1\mu_0$, and $\mu = \mu_0$, where $\mu_0 = 1$ cm^{-1} [21,46], the optimal value of L is 0.4–1.5 cm. With the above parameters, here we will focus on the quantum state distribution of two outputs for both $\mathcal{PT}$-symmetry and $\mathcal{PT}$-broken cases.

We first consider the situation of single photon input, i.e., $|\psi\rangle_{in} = |0, 1\rangle$ and $|1, 0\rangle$ [40]. In the case of $\mathcal{PT}$ symmetry, the photons tend to symmetrically distribute in two waveguides, while in the $\mathcal{PT}$-broken case, whatever inputting one photon from which waveguide, the photons are likely to output from the dominant waveguide, which is in agreement with classical optical experiments where most of the energy is locating in the dominant mode [21]. Then the situation of multiphoton input is explored, i.e., $|\psi\rangle_{\text{in}} = |0, N\rangle$ and $|N, 0\rangle$ [40]. Once

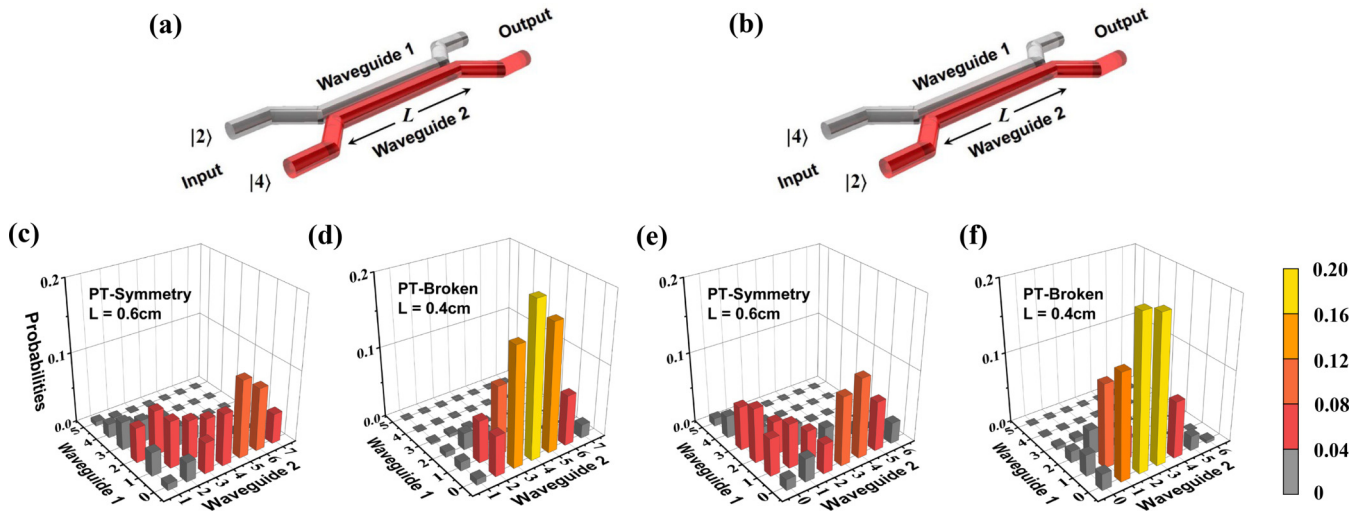

FIG. 3. Schematics of coupled waveguides with input Fock states (a) $|2, 4\rangle$ for (c), (d) and (b) $|4, 2\rangle$ for (e), (f). Probability distributions of output states for (c), (e) $\mathcal{PT}$ symmetry at $L = 0.6$ cm and (d), (f) $\mathcal{PT}$ broken at $L = 0.4$ cm. Other parameters are the same as those in Figs. 2(b) and 2(c).

again, after EP, most of the photons (or the output states with large probability) are concentrating on the dominant waveguide due to the joint effect of quantum interference and $\mathcal{PT}$ broken.

Also, because of the photon concentration of $\mathcal{PT}$ broken, the Fock state $|P\rangle$ with $P > M, N$ appears when $|\psi\rangle_{\text{in}} = |M, N\rangle$. So, the beam splitter with this kind of $\mathcal{PT}$ broken can be used to prepare the high number Fock state. Now, we take the input states of $|\psi\rangle_{\text{in}} = |2, 4\rangle$ and $|4, 2\rangle$ as examples. As shown in Figs. 3(c) and 3(e), in the case of $\mathcal{PT}$ symmetry [yellow star in Fig. 1(b)], the photon number distribution at $L = 0.6$ cm is dispersed due to exchanging between two waveguides. The mean photon numbers are $\langle\hat{n}_1\rangle = 1.2$ and $\langle\hat{n}_2\rangle = 3.3$ (input $|2, 4\rangle$) and $\langle\hat{n}_1\rangle = 1.1$ and $\langle\hat{n}_2\rangle = 2.3$ (input $|4, 2\rangle$), while in the $\mathcal{PT}$ broken [red star in Fig. 1(b)], at $L = 0.4$ cm, most photons are gathered in the dominant waveguide with large probability distributions of high number Fock state such as $|5\rangle$ [Figs. 3(d) and 3(f)], corresponding to $\langle\hat{n}_1\rangle = 0.4$ and $\langle\hat{n}_2\rangle = 2.0$ (input $|2, 4\rangle$) and $\langle\hat{n}_1\rangle = 0.3$ and $\langle\hat{n}_2\rangle = 3.7$ (input $|4, 2\rangle$). If the input state is another Fock state $|M, N\rangle$ with the total number of photons $M + N < 10$, the same result is obtained [40]. Finally, owing to the quantum jump effects, for the same point in the $\mathcal{PT}$-phase diagram, such as the red star in Fig. 1(b), the quantum state distributions can be optimized through adjusting the loss and gain of two waveguides [40].

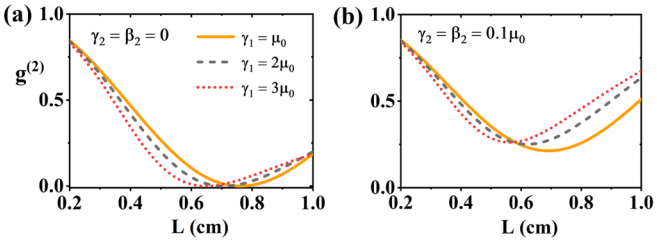

FIG. 4. Quantum jump effect on HOM interference in non-Hermitian beam splitter. $g^{(2)}$ as a function of propagation distance L (a) without gain and (b) with gain. Here, $\beta_1 = 0$, $\mu = \mu_0$ and the input state is $|1, 1\rangle$. The yellow(solid)/gray(dashed)/red(dotted) curves correspond to the yellow/gray/red star in Fig. 1(b), representing $\mathcal{PT}$ symmetry/EP/$\mathcal{PT}$ broken.

Then, the quantum jump effect on Hong-Ou-Mandel (HOM) interference [47] is explored. The input is $|\psi\rangle_{\text{in}} = |1, 1\rangle$ and $g^{(2)} = \langle\hat{a}_1^\dagger\hat{a}_2^\dagger\hat{a}_2\hat{a}_1\rangle/\langle\hat{a}_1^\dagger\hat{a}_1\rangle\langle\hat{a}_2^\dagger\hat{a}_2\rangle$. For the same point in the phase diagram, if without gain, whenever for $\mathcal{PT}$-symmetric or broken, the minimum of $g^{(2)}$ can always reach zero [Fig. 4(a)] [46]. While the gain is added, whether the loss exists or not, this value generally cannot be zero and become larger with increasing the gain [Fig. 4(b)]. Even though the values of loss and gain in the second waveguide are the same, they not only cannot cancel each other as what was found in the classical case, but also lead to more noise. This means that, owing to different quantum jump effects, gain cannot compensate loss in quantum $\mathcal{PT}$ systems.

Moreover, as for coherent states, gain brings noise to the output states, while loss does not [40], which further confirms the difference between loss and gain. In experiment, quantum noise can be estimated from balanced homodyne measurement [48].

Summary. By considering the quantum jump, we have analytically obtained the quantum $\mathcal{PT}$-phase diagram with the steady-state regime in non-Hermitian photonic structures. We have defined an exchange operator to characterize the $\mathcal{PT}$-symmetry phase and $\mathcal{PT}$-broken phase. Based on this phase diagram, in the coupled waveguide structure, we have engineered the multiphoton quantum state especially on the $\mathcal{PT}$-broken regime and discussed the HOM effects with gain. Different quantum jump effects of gain and loss prevent them from compensating for each other and further give rise to an imperfect HOM effect. The established theory can be extended to study many related quantum behaviors, such as gain saturation effect, quantum entanglement, and continuous variable states, and may have potential applications in quantum state preparation, quantum interferences, and logic operations in non-Hermitian photonic systems.

Acknowledgments. This work was supported by the Innovation Program for Quantum Science and Technology (2021ZD0301500) and the National Natural Science Foundation of China (11974032).

[1] C. M. Bender and S. Boettcher, Real spectra in non-Hermitian Hamiltonians having $\mathcal{PT}$ symmetry, Phys. Rev. Lett. **80**, 5243 (1998).
[2] A. Mostafazadeh, Quantum brachistochrone problem and the geometry of the state space in pseudo-Hermitian quantum mechanics, Phys. Rev. Lett. **99**, 130502 (2007).
[3] H. Schomerus, Quantum noise and self-sustained radiation of $\mathcal{PT}$-symmetric systems, Phys. Rev. Lett. **104**, 233601 (2010).
[4] T. Prosen, $\mathcal{PT}$-symmetric quantum liouvillean dynamics, Phys. Rev. Lett. **109**, 090404 (2012).
[5] Z. H. Musslimani, K. G. Makris, R. El-Ganainy, and D. N. Christodoulides, Optical solitons in $\mathcal{PT}$ periodic potentials, Phys. Rev. Lett. **100**, 030402 (2008).
[6] S. Longhi, Bloch oscillations in complex crystals with $\mathcal{PT}$ symmetry, Phys. Rev. Lett. **103**, 123601 (2009).
[7] A. Y. Song, X. Q. Sun, A. Dutt, M. Minkov, C. Wojcik, H. Wang, I. A. D. Williamson, M. Orenstein, and S. Fan, $\mathcal{PT}$-symmetric topological edge-gain effect, Phys. Rev. Lett. **125**, 033603 (2020).
[8] Y. Li, C. Liang, C. Wang, C. Lu, and Y.-C. Liu, Gain-loss-induced hybrid skin-topological effect, Phys. Rev. Lett. **128**, 223903 (2022).
[9] Z. Zhang, Y. Zhang, J. Sheng, L. Yang, M.-A. Miri, D. N. Christodoulides, B. He, Y. Zhang, and M. Xiao, Observation of parity-time symmetry in optically induced atomic lattices, Phys. Rev. Lett. **117**, 123601 (2016).
[10] L. Ding, K. Shi, Q. Zhang, D. Shen, X. Zhang, and W. Zhang, Experimental determination of $\mathcal{PT}$-symmetric exceptional points in a single trapped ion, Phys. Rev. Lett. **126**, 083604 (2021).
[11] Y. Yang, H. Jia, Y. Bi, H. Zhao, and J. Yang, Experimental demonstration of an acoustic asymmetric diffraction grating based on passive parity-time-symmetric medium, Phys. Rev. Appl. **12**, 034040 (2019).
[12] M. Sakhdari, M. Hajizadegan, Q. Zhong, D. N. Christodoulides, R. El-Ganainy, and P.-Y. Chen, Experimental observation of *pt* symmetry breaking near divergent exceptional points, Phys. Rev. Lett. **123**, 193901 (2019).
[13] T. Biesenthal, M. Kremer, M. Heinrich, and A. Szameit, Experimental realization of $\mathcal{PT}$-symmetric flat bands, Phys. Rev. Lett. **123**, 183601 (2019).
[14] L. Xiao, K. Wang, X. Zhan, Z. Bian, K. Kawabata, M. Ueda, W. Yi, and P. Xue, Observation of critical phenomena in parity-time-symmetric quantum dynamics, Phys. Rev. Lett. **123**, 230401 (2019).
[15] T. Wu, J. A. Izaac, Z.-X. Li, K. Wang, Z.-Z. Chen, S. Zhu, J. B. Wang, and X.-S. Ma, Experimental parity-time symmetric quantum walks for centrality ranking on directed graphs, Phys. Rev. Lett. **125**, 240501 (2020).
[16] L. Xiao, T. Deng, K. Wang, Z. Wang, W. Yi, and P. Xue, Observation of non-bloch parity-time symmetry and exceptional points, Phys. Rev. Lett. **126**, 230402 (2021).
[17] R. El-Ganainy, K. G. Makris, D. N. Christodoulides, and Z. H. Musslimani, Theory of coupled optical $\mathcal{PT}$-symmetric structures, Opt. Lett. **32**, 2632 (2007).
[18] M.-A. Miri and A. Alù, Exceptional points in optics and photonics, Science **363**, eaar7709 (2019).
[19] L. Feng, R. El-Ganainy, and L. Ge, Non-hermitian photonics based on parity-time symmetry, Nat. Photon. **11**, 752 (2017).
[20] A. Guo, G. J. Salamo, D. Duchesne, R. Morandotti, M. Volatier-Ravat, V. Aimez, G. A. Siviloglou, and D. N. Christodoulides, Observation of $\mathcal{PT}$-symmetry breaking in complex optical potentials, Phys. Rev. Lett. **103**, 093902 (2009).
[21] C. E. Rüter, K. G. Makris, R. El-Ganainy, D. N. Christodoulides, S. Mordechai, and K. Detlef, Observation of parity-time symmetry in optics, Nat. Phys. **6**, 192 (2010).
[22] L. Chang, X. Jiang, S. Hua, C. Yang, J. Wen, L. Jiang, G. Li, G. Wang, and M. Xiao, Parity-time symmetry and variable optical isolation in active-passive-coupled microresonators, Nat. Photon. **8**, 524 (2014).
[23] B. Peng, Ş. K. Özdemir, F. Lei, F. Monifi, M. Gianfreda, G. Long, S. Fan, F. Nori, C. M. Bender, and L. Yang, Parity-time-symmetric whispering-gallery microcavities, Nat. Phys. **10**, 394 (2014).
[24] M. Lawrence, N. Xu, X. Zhang, L. Cong, J. Han, W. Zhang, and S. Zhang, Manifestation of $\mathcal{PT}$ symmetry breaking in polarization space with terahertz metasurfaces, Phys. Rev. Lett. **113**, 093901 (2014).
[25] Z. Lin, H. Ramezani, T. Eichelkraut, T. Kottos, H. Cao, and D. N. Christodoulides, Unidirectional invisibility induced by $\mathcal{PT}$-symmetric periodic structures, Phys. Rev. Lett. **106**, 213901 (2011).
[26] L. Feng, M. Ayache, J. Huang, Y. Xu, M. Lu, Y. Chen, Y. Fainman, and A. Scherer, Nonreciprocal light propagation in a silicon photonic circuit, Science **333**, 729 (2011).
[27] J. Wiersig, Enhancing the sensitivity of frequency and energy splitting detection by using exceptional points: Application to microcavity sensors for single-particle detection, Phys. Rev. Lett. **112**, 203901 (2014).
[28] B. Peng, Ş. K. Özdemir, S. Rotter, H. Yilmaz, M. Liertzer, F. Monifi, C. M. Bender, F. Nori, and L. Yang, Loss-induced suppression and revival of lasing, Science **346**, 328 (2014).
[29] L. Feng, Z. J. Wong, R.-M. Ma, Y. Wang, and X. Zhang, Single-mode laser by parity-time symmetry breaking, Science **346**, 972 (2014).
[30] B. Peng, Ş. K. Özdemir, M. Liertzer, W. Chen, J. Kramer, H. Ylmaz, J. Wiersig, S. Rotter, and L. Yang, Chiral modes and directional lasing at exceptional points, Proc. Natl. Acad. Sci. USA **113**, 6845 (2016).
[31] I. I. Arkhipov, A. Miranowicz, O. Di Stefano, R. Stassi, S. Savasta, F. Nori, and S. K. Özdemir, Scully-lamb quantum laser model for parity-time-symmetric whispering-gallery microcavities: Gain saturation effects and nonreciprocity, Phys. Rev. A **99**, 053806 (2019).
[32] S. Vashahri-Ghamsari, B. He, and M. Xiao, Effects of gain saturation on the quantum properties of light in a non-Hermitian gain-loss coupler, Phys. Rev. A **99**, 023819 (2019).
[33] F. Minganti, A. Miranowicz, R. W. Chhajlany, and F. Nori, Quantum exceptional points of non-Hermitian Hamiltonians

and liouvillians: The effects of quantum jumps, Phys. Rev. A **100**, 062131 (2019).

[34] I. I. Arkhipov, A. Miranowicz, F. Minganti, and F. Nori, Quantum and semiclassical exceptional points of a linear system of coupled cavities with losses and gain within the scully-lamb laser theory, Phys. Rev. A **101**, 013812 (2020).

[35] I. I. Arkhipov, A. Miranowicz, F. Minganti, and F. Nori, Liouvillian exceptional points of any order in dissipative linear bosonic systems: Coherence functions and switching between $\mathcal{PT}$ and anti-$\mathcal{PT}$ symmetries, Phys. Rev. A **102**, 033715 (2020).

[36] F. Roccati, A. Purkayastha, G. M. Palma, and F. Ciccarello, Quantum correlations in dissipative gain-loss systems across exceptional points, Eur. Phys. J. Spec. Top. **232**, 1783 (2023).

[37] M. Sargent III, M. O. Scully, and W. E. Lamb, Jr., *Laser Physics* (Addison-Wesley Publishing Company, Redwood City, CA, 1974).

[38] G. Lindblad, On the generators of quantum dynamical semigroups, Commun. Math. Phys. **48**, 119 (1976).

[39] S. Scheel and A. Szameit, $\mathcal{PT}$-symmetric photonic quantum systems with gain and loss do not exist, Europhys. Lett. **122**, 34001 (2018).

[40] See Supplemental Material at http://link.aps.org/supplemental/10.1103/PhysRevA.109.L041503 for derivation of the evolution equation, steady state, properties of Liouvillian, $\mathcal{PT}$ phase characterization, and quantum state engineering.

[41] Q. Zhang, Y. Ma, Q. Liu, X. Zhang, Y. Jia, L. Tong, Q. Gong, and Y. Gu, Gain-gain and gain-lossless $\mathcal{PT}$-symmetry broken from $\mathcal{PT}$-phase diagram, J. Opt. **52**, 2239 (2023).

[42] S. M. Barnett, J. Jeffers, A. Gatti, and R. Loudon, Quantum optics of lossy beam splitters, Phys. Rev. A **57**, 2134 (1998).

[43] T. Roger, S. Restuccia, A. Lyons, D. Giovannini, J. Romero, J. Jeffers, M. Padgett, and D. Faccio, Coherent absorption of N00N states, Phys. Rev. Lett. **117**, 023601 (2016).

[44] B. Vest, M.-C. Dheur, É. Devaux, A. Baron, E. Rousseau, J.-P. Hugonin, J.-J. Greffet, G. Messin, and F. Marquier, Anti-coalescence of bosons on a lossy beam splitter, Science **356**, 1373 (2017).

[45] J. E. Davis and D. O. Güney, Effect of loss on linear optical quantum logic gates, J. Opt. Soc. Am. B **38**, C153 (2021).

[46] F. Klauck, L. Teuber, M. Ornigotti *et al.*, Observation of $\mathcal{PT}$-symmetric quantum interference, Nat. Photon. **13**, 883 (2019).

[47] C. K. Hong, Z. Y. Ou, and L. Mandel, Measurement of subpicosecond time intervals between two photons by interference, Phys. Rev. Lett. **59**, 2044 (1987).

[48] A. Furusawa, *Quantum States of Light* (Springer, New York, 2015).